Application of Laser-Induced Thermal Acoustics
to a High-Lift Configuration

Luther N. Jenkins[*], Roger C. Hart, R. Jeffrey Balla, Greg C. Herring,
Mehdi R. Khorrami, and Meelan M. Choudhari
National Aeronautics and Space Administration
Langley Research Center
Hampton, Virginia 23681-2199 USA

ABSTRACT

Laser-Induced Thermal Acoustics (LITA) has been used to measure the flow field in the slat region of a two-dimensional, high-lift system in the NASA Langley Basic Aerodynamics Research Tunnel (BART). Unlike other point-wise, non-intrusive measurement techniques, LITA does not require the addition of molecular or particulate seed to the flow. This provides an opportunity to obtain additional insight and detailed flow-field information in complex flows where seeding may be insufficient or detection is problematic. Based on the successful use of LITA to measure the flow over a backward-facing step, the goal of this study was to further evaluate the technique by applying it to a more relevant and challenging flow field such as the slat wake on a high-lift system. Streamwise velocities were measured in the slat wake and over the main element at 11.3 degrees angle of attack and a freestream Mach Number of 0.17. The single-component LITA system is described and velocity profiles obtained using LITA are compared to profiles obtained using two-dimensional, Digital Particle Image Velocimetry (DPIV) and a steady, Reynolds-Averaged Navier-Stokes (RANS) flow solver for the same configuration. The normalized data show good agreement where the number of measurement locations had sufficient density to capture the pertinent flow phenomena.

Keywords: LITA, PIV, High-Lift, Wake Measurements, Non-Intrusive Measurement Techniques, Leading-Edge Slat

1. INTRODUCTION

Computational methods are considered to be the most effective mechanism for establishing an integrated approach to aircraft design that incorporates fuselage components, engine components, cruise wing configurations, and high-lift systems. One of the goals of the NASA Airframe Systems Concept-to-Test (ASCOT) Research Program is to improve the speed and accuracy of design tools that can be used for this purpose by considering barrier technology issues for computational methods. This effort has placed great emphasis on establishing databases for validating the computational methods and understanding the flow physics. The flow physics associated with multi-element, high-lift wings and airfoils for transport airplanes presents an extreme challenge to both experimental and computational aerodynamicists. Figure 1 identifies the myriad of flow phenomena associated with a high-lift system, each of which has to be modeled efficiently and accurately by the computational method to properly assess aerodynamic performance and environmental effects.

The accuracy of computational methods can only be determined through detailed comparisons with data acquired from wind tunnel or flight experiments. According to Bradley[1], the experimental databases used in these comparisons must include surface quantities, but also detailed measurements of fluid and thermals throughout the flow region of interest. Over the past 30 years, non-intrusive, measurement techniques such as Laser Doppler Velocimetry (LDV), Doppler Global Velocimetry (DGV), and Particle Image Velocimetry (PIV) have been developed to complement traditional techniques such as flow visualization, surface pressures, forces and moments, pressure probes, and hot-wire anemometry to provide greater insight into complex flows and establish detailed datasets. However, a limitation often encountered when using non-intrusive measurement techniques is that most require the addition of molecular or particulate seed to

---

[*] l.n.jenkins@larc.nasa.gov; phone 1 757 864-8026; fax 1 757 864-8677

the flow field. In many cases, a large part of the experimental effort is spent devising ways to properly inject seed into the flow and achieve sufficient seed density in the regions where measurements are to be made. This is especially true in regions of flow separation or flow reversals. In addition to seed injection and density, particle size is also a consideration when using particle-based techniques. The particle size must be sufficient for detection but small enough to follow the streamlines in the flow. Since no single measurement technique has established itself as the panacea, experimentalists often utilize redundant measurement techniques for data corroboration and to account for limitations in a given technique.
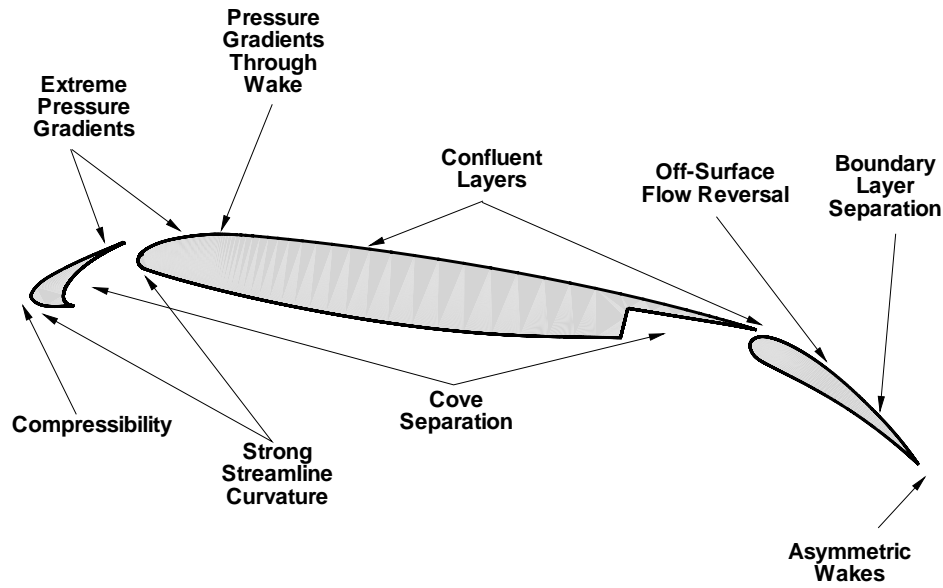

Figure 1. Flow features associated with a multi-element, high-lift wing.

Over the past ten years, Laser-Induced Thermal Acoustics (LITA) has emerged as a measurement technique that appears to address many of the issues associated with particle-based techniques. LITA is essentially a "seedless" diagnostic tool capable of measuring temperature and velocity in a variety of flow fields. Prior research by Hart, et. al.[2] has shown that LITA compares quite well with LDV when applied to the flow over a backward-facing step. Figure 2 shows a profile measured through the free shear layer behind the step using the two techniques. Based on the success of this work, it was decided to apply the LITA technique to a more challenging and complex aerodynamic flow such
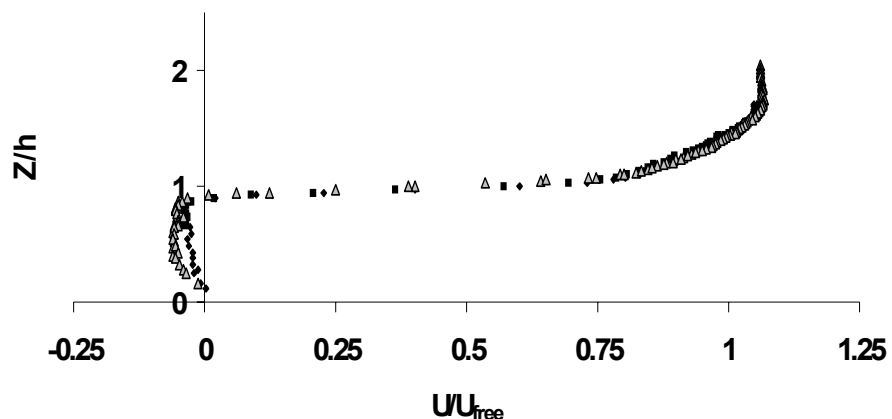

Figure 2. Mean velocity profiles at x/h = 0.52 taken using LITA (dark symbols) and LDV (gray triangles).

as the slat wake of a two-dimensional, high-lift system. This paper describes the LITA system developed for this particular application and compares LITA data with results obtained on the same configuration using PIV and a Computational Fluid Dynamics (CFD) flow solver.

2. LASER-INDUCED THERMAL ACOUSTICS

The use of a laser-induced grating for flow diagnostics was suggested at least as early as Eichler[3]. Cummings[4-6] reported the first demonstration of LITA for gas-phase thermal diffusivity and speed of sound measurements using seeded NO_2 to enhance signal levels. Other workers have investigated the use of LITA thermometry in air[7-9], flames[10], and supersonic flows[11]. LITA velocimetry has been demonstrated using a narrow-band laser and high-finesse Fabry-Perot etalon[12], homodyne detection[13], and several approaches to heterodyne detection[14-16]. Here we present a significantly more stable approach to heterodyne detection which can form the basis for a practical, rugged, robust LITA velocimeter.

A LITA measurement involves four steps: 1) creation of acoustic waves in the medium using a short-pulse pump laser; 2) "probing" the moving acoustic waves using a long-pulse or CW probe laser beam; 3) detection of the light scattered by Bragg diffraction; and 4) analysis of the resulting Doppler shifts to determine temperature and velocity. The process is reminiscent of LDV, with the acoustic waves generated by the pump laser taking the place of a seed particle. Two consequences of this 'self-seeding' are 1) measurements can be made in any portion of the flow accessible to the beams, and 2) since the data rate is determined by the firing of the pump laser and is totally independent of flow conditions, there is no velocity bias.
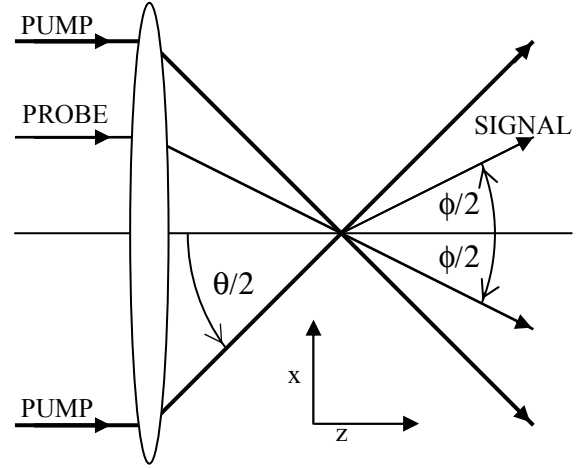

Figure 3. The pump beams cross at angle θ producing an acoustic grating. Probe light incident at φ/2 is diffracted into the signal beam. Z is parallel to the optic axis, while x lies in the plane of the beams.

2.1 Pump Step

Figure 3 shows a schematic of the optical arrangement for the system. The beam from a short-pulse, high-intensity laser (e.g. Q-switched Nd:YAG) is split into two parallel, equal intensity beams with path lengths matched to within the coherence length. A lens causes the beams of wavelength λ_{PUMP} to cross at angle θ and focus at a common point where interference fringes of period $\Lambda = \lambda_{PUMP}/2\sin(\theta/2)$ form along the x direction. In this application air is the medium, the pump light is not resonant with any absorptive transition. However, electrostriction creates a pressure field proportional to the intensity, which is the driving term for the launch of a pair of counter-propagating acoustic waves of wavelength Λ[17]. The acoustic frequency in angular units measured in a frame at rest with respect to the air is then $\omega_B = 2\pi V_{SOUND}/\Lambda$, where V_{SOUND} is the speed of sound. The intensity of the acoustic waves is estimated to be less than 100 dB, so the waves represent a negligible perturbation to any aerodynamic phenomena.

If the pump light is resonant with an absorptive transition in the medium, the efficiency of the pumping process can be greatly increased provided the absorbed energy is thermalized on a time scale short in comparison with the acoustic period. This approach was not pursued because 1) it requires the introduction of a seed species into the flow, and most optically suitable seed molecules are chemically reactive or present other risks to equipment or personnel, and 2) the pump laser must be in general tuned onto the transition, which requires a tunable laser and possibly some means of locking the laser onto the transition. (However, both I_2 and NO_2 are resonant with the 2nd Nd:YAG harmonic). Non-resonant pumping provides adequate signal levels at ambient conditions with a heterodyne detection scheme and is both simpler to implement and more broadly applicable.

2.2 Probe Step

LITA is capable of both thermometry and velocimetry measurements using the fact that the polarization induced in a medium by an incident light wave is proportional to the density. If a sinusoidal density modulation of period Λ (the acoustic wave) is illuminated at angle $\phi/2$ (Fig. 3) with light of wavelength λ_{PROBE} and $\Lambda = \lambda_{PROBE}/2\sin(\phi/2)$, the resulting polarization distribution will generate a propagating light beam at angle $\phi/2$. This is Bragg diffraction by the acoustic wave, also known as the acoustic grating. The relationship,

$$\frac{\lambda_{PUMP}}{2\sin(\theta/2)} = \Lambda = \frac{\lambda_{PROBE}}{2\sin(\phi/2)}, \tag{1}$$

requires that the probe be phase-matched to the grating created by the pump laser. For a plane-wave model based on beams of infinite transverse extent, phase matching is a delta function in angle. For focused geometries where the gratings may be only a few tens of fringes wide, phase matching is much more relaxed and requires only approximate adjustment.

In the geometry shown in Fig. 3, the gratings move at $\pm V_{SOUND}$ with respect to the medium in the x-direction. Additionally, there may be a component of a convective flow field in the x-direction, V_{FLOW}. If the overlapping signal beams with Doppler shifts of $\Delta\omega_- = (2\pi/\Lambda)(V_{FLOW} - V_{SOUND})$ and $\Delta\omega_+ = (2\pi/\Lambda)(V_{FLOW} + V_{SOUND})$ are incident on a detector, a modulation of the photocurrent at the difference or beat frequency, $2\omega_B$, is observed. Since $2\omega_B$ is proportional to the difference in the x-component of the velocities of the two acoustic gratings, it is independent of V_{FLOW}. Thus, if Λ is known, the speed of sound can be obtained and used to compute temperature, provided that the composition of the medium is known. Reference 8 presents an extensive laboratory study of LITA thermometry in air where a reference cell was employed to avoid errors and uncertainties in the calibration of Λ. In this setup, a small fraction of the converging pump and probe beams was split off and allowed to intersect in a cell containing air of known temperature. Comparison of the observed beat frequencies from the test and reference cells then gave the temperature in the test cell independently of Λ.

For velocity measurements, the two gratings moving at $V_{FLOW} + V_{SOUND}$ and $V_{FLOW} - V_{SOUND}$ created in the lab frame permit V_{FLOW} and V_{SOUND} to be determined independently. If a beam (termed the local oscillator) at the frequency of the probe is introduced collinear to the signal beams, the time-varying intensity on the detector is

$$I(t) \propto \sqrt{I_{LO}I_{SIGNAL}}(\cos(\Delta\omega_+ t) + \cos(\Delta\omega_- t)) + I_{SIGNAL}\cos(2\omega_B t), \tag{2}$$

where I_{LO} and I_{SIGNAL} are the intensities of the local oscillator and signal beams. Spectral analysis (e.g. discrete Fourier transform) of a real-valued time series cannot retrieve $\Delta\omega_+$ or $\Delta\omega_-$, but only $|\Delta\omega_+|$ and $|\Delta\omega_-|$. If $V_{FLOW} < V_{SOUND}$, then

$$|V_{FLOW}| = \frac{1}{2}\left(\frac{\Lambda}{2\pi}\right)\left||\Delta\omega_+| - |\Delta\omega_-|\right| \tag{3}$$

and

$$V_{SOUND} = \frac{1}{2}\left(\frac{\Lambda}{2\pi}\right)\left(|\Delta\omega_+| + |\Delta\omega_-|\right). \tag{4}$$

Note that Mach number can then be found independently of Λ using the following equation.

$$M = \frac{|V_{FLOW}|}{V_{SOUND}} = \frac{\left||\Delta\omega_+| - |\Delta\omega_-|\right|}{|\Delta\omega_+| + |\Delta\omega_-|} \tag{5}$$

For measurements in an isothermal, incompressible flow, V_{SOUND} may be determined from the known flow temperature and V_{FLOW} found without other calibration. If the flow is not isothermal, a reference cell may be used or Λ may be calibrated by measuring $2\omega_B$ at known temperature. Problems associated with the use of a collinear, local oscillator as well as the determination of flow direction are addressed using grating demodulation. For a detail treatment of the grating demodulation used in this application, the reader is directed to Reference 19.

3. EXPERIMENTAL APPARATUS AND METHODS

3.1 Test Facility

The experiment was conducted in the NASA-Langley Basic Aerodynamics Research Tunnel (BART). This tunnel is a subsonic, atmospheric wind tunnel used to investigate the fundamental characteristics of complex flow fields and to acquire detailed data for the development and validation of CFD models and methods. The tunnel has a closed test section with a height of 0.711 meters, a width of 1.016 meters, and a length of 3.048 meters. The maximum velocity entering the test section is approximately 57 m/s. This equates to a unit Reynolds Number (Re/m) of 3.64 million and produces a turbulence level of 0.09%. Additional information about the BART can be found in References 20, 21, and 22.
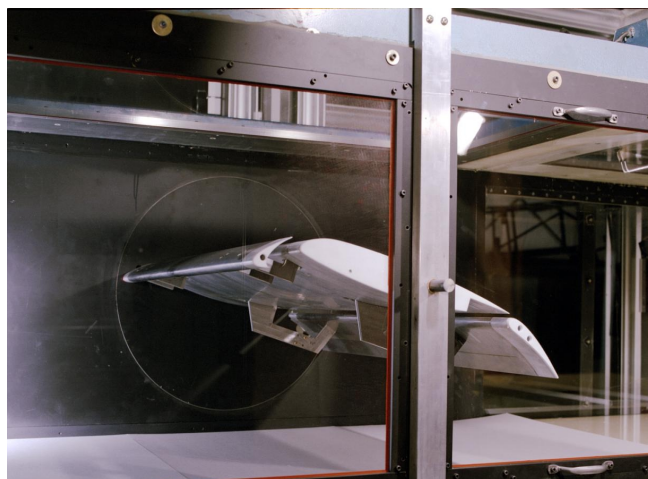
3.2 Model

The McDonnell Douglas Aerospace (MDA) 30P-30N, high-lift configuration was selected as a representative

Figure 4. Douglas (MDA) high-lift model in the Basic Aerodynamics Research Tunnel.

high-lift system for this application. This particular geometry has been used in studies by Klausmeyer, et. al.[23] to examine separation control using micro-vortex generators on the flap and by Paschal, et. al.[24] to characterize unsteadiness in the slat wake. The model, shown in Figure 4, has a nested chord of 0.46 meters and consists of a main element, slat, and single element flap that span the tunnel width. The main element is supported by a dowel/slip bearing on one wall and attached to a turntable on the other wall. For this entry, a small glass window was installed in the turntable to provide the "line-of-sight" access required by LITA. An actuator was used to rotate the turntable and set the angle of attack. Brackets are used to attach the slat and flap to the main element and also to set the gap, overhang, and deflection angles.

The model is instrumented with a single, chordwise row of pressure orifices on the centerline of the three elements and two spanwise rows of pressure orifices on the main element and flap, respectively. Although sidewall blowing was not used as in Reference 24, the pressures measured by spanwise rows were used to verify the quasi-two-dimensionality of the flow in the measurement region.

3.3 Experimental Techniques

3.3.1 LITA

The one-component LITA velocimeter used in this investigation was non-resonant and comprised of transmitter and receiver modules that contained the lasers and optics. Each module measured approximately 0.61 meters long by 0.30 meters wide by 0.41 meters high and weighed less than 45.35 kilograms each. They were located on opposite sides of the test section and mounted to a three degree-of-freedom traverse system surrounding the tunnel. This mounting arrangement permitted the entire system to be traversed while maintaining the optical alignment.

The transmit module featured a 800 mJ/pulse, Q-switched Nd:YAG laser with a 10 Hz repetition rate flash-lamp and an output wavelength of 1064 nm. The laser head was sealed and employed hard-mounted (non-adjustable) optics. The

probe laser was diode pumped and provided 10 W of CW 532 nm light. The probe laser head was also sealed and non-adjustable. Both lasers operated using 115 VAC and neither required an external cooling water supply. The pump and probe laser heads were demountable from the transmitter module so the lasers could be transported separately. The pump and probe beams were focused and crossed by a 750 mm focal length plano-convex lens. The probe focal spot diameter was measured to be about 300 μm, while the pump spot diameter was 2.5 mm giving a pump intensity of approximately 2 x 10^9 W/cm^2. The pump crossing angle was 1.4° giving $\omega_B \approx 7.8$ MHz. The large pump spot size is due to the multiple transverse mode output of the pump laser, and in fact, a 1.5:1 telescope was employed to enlarge the pump beam before splitting and focusing to reduce the focal spot diameter.

In addition to the grating demodulation optics, the receiver contained the optics for the Focal Plane Camera (FPC). A very small fraction of the pump and probe beams was split off and brought to a focus; this focus was then re-imaged onto a CCD array using a microscope objective. The purpose of this step was to allow real-time monitoring of the relative positions of the probe and the two pump beams at the beam crossing point. Slight adjustments in the beam positions were required during data acquisition, especially to the pump beam overlap due to the multiple transverse mode output of the pump laser. Inspection of the beam positions as well as the resulting signal greatly eases this process.

The tunnel traverse system was calibrated with respect to the model by intersecting the probe beam with the slat trailing edge. Figure 5 identifies the 8 data stations and shows the location of each LITA measurement with respect to the model. The data stations consist of 2 locations upstream and 3 locations downstream of the slat trailing edge, 2 detailed scans perpendicular to the slat trailing edge through the wake, and one horizontal scan above the slat trailing edge and leading edge of the main element. At each point along the 8 traverses, 500 LITA shots were acquired. Individual waveforms were acquired with a high-speed digitizer and stored on a PC hard disk. Offline processing consisted primarily of fitting a model described in References 2 and 19 to the time domain data using Pronys' method and using the recovered values of $\Delta\omega_+$ and $\Delta\omega_-$ to find Mach number. Knowledge of the free-stream air temperature from a thermocouple probe then allowed computation of the flow velocity. The uncertainty

Figure 5. LITA and PIV measurement locations.

of the velocities measured by LITA is estimated to be less than 2 m/s. All of the measurements were made at a free stream velocity of 56 m/s, Mach Number of 0.17, and 11.3 degrees angle of attack.
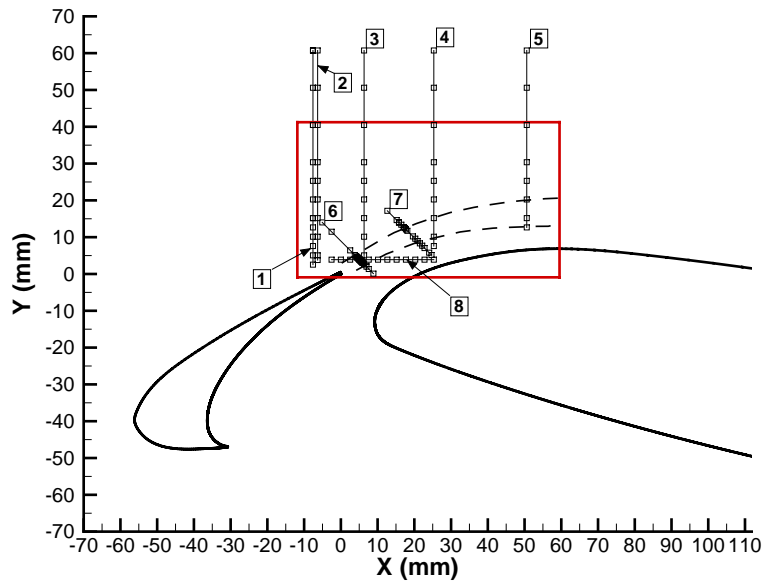
3.3.2 PIV

Particle Image Velocimeter (PIV) data was acquired during a separate wind tunnel test at the same freestream conditions and angle of attack for comparison with the LITA data. A single, high-resolution, video camera with a sensor size of 1360 pixels by 1024 pixels was used to acquire the images. The camera was mounted to the tunnel traverse system along with the laser and light-sheet optics. A 1.5 mm thick light sheet was generated using a pulsed, frequency-doubled, 200mJ Nd-YAG laser operated at 5 Hz. The light sheet was aligned perpendicular to the model upper surface and parallel to the model centerline. The measurements were made in a plane located near the leading edge of the main

element and approximately 101.6 mm away from the model centerline where the model was coated with a fluorescent coating to reduce the flare from the surface. Figure 5 shows the PIV image area relative to the LITA measurement locations. The camera was focused on this plane using a 50 mm macro lens to produce a field-of-view 80 mm wide by 60 mm tall. The entire room housing the tunnel was seeded with 0.5-1.5 micron particles produced by a theatrical fog machine. Each acquisition sequence consisted of 500 image pairs that were processed using the algorithm described in Reference 25 and averaged to obtain mean velocities. The measurement volume based on a 24 pixel by 24 pixel interrogation area was estimated to be 1.4 mm^2. The uncertainty in the PIV data is estimated to be ±3 m/s.

3.4 Computational Technique

The computation results to be compared with the LITA data in the following sections were computed using CFL3D[26], a flow solver developed at NASA Langley Research Center. The CFL3D code solves the compressible, thin-layer, Reynolds-averaged Navier-Stokes equations using a finite volume formulation. Menter's two-equation, Shear Stress Transport (SST), k-ω turbulence model[27] was selected to conduct the present computations. The structured grid consists of 698K mesh points distributed over 22 blocks. Nearly sixty percent of the points were clustered in the vicinity of the slat and the leading edge of the main element where extremely fine meshes are used. To curb the total number of grid points, patching strategy was utilized to prevent unwanted propagation of the fine grid cells to other regions.

The 2D computations are performed in a fully turbulent mode and no effort was made to model the transitional flow regions on the leading edge slat. To ensure a direct comparison with the measurements, the entire test section of the BART facility was modeled and included in the simulations. The tunnel walls, however, were treated as inviscid.

4. RESULTS AND DISCUSSION

To assess the ability of LITA to measure the flow over a high-lift configuration, streamwise velocities from the PIV and CFD datasets were extracted at the same locations as the LITA measurements and compared with LITA profiles in Figures 6-13. The data and all dimensions are referenced to the coordinate axis system of the wind tunnel. Although other statistical parameters can be calculated from the LITA and PIV datasets, only the time-averaged velocities will be discussed. To quantify the relative agreement between the LITA, PIV, and CFD, the percent difference between the techniques is defined as

$$Percent\ Difference_{PIV} = \frac{(U/U_\infty)_{LITA} - (U/U_\infty)_{PIV}}{(U/U_\infty)_{PIV}} \times 100\% \tag{6}$$

and

$$Percent\ Difference_{CFD} = \frac{(U/U_\infty)_{LITA} - (U/U_\infty)_{CFD}}{(U/U_\infty)_{CFD}} \times 100\% , \tag{7}$$

where U is the velocity measured but the specified technique and U_∞ is the velocity of the tunnel free stream. Table 1 shows the maximum and minimum percent difference between LITA, PIV, and CFD for each measurement location and will be referenced during the discussion in the following sections.

4.1 Slat Upper Surface

When conducting a flow physics investigation, it is typically good practice to measure the velocity immediately upstream of the phenomenon being investigated. Data measured at this location is necessary when comparing computational results or different experimental techniques to insure that the flow field producing the phenomenon is the same. Since this investigation focused on the slat wake, velocity measurements were made on the slat upper surface upstream of the trailing edge. Figures 6 and 7 compare the normalized, streamwise velocity at Station 1 (x = -7.39 mm)

Profile	Minimum Percent Difference (LITA vs. PIV)	Maximum Percent Difference (LITA vs. PIV)	Minimum Percent Difference (LITA vs. CFD)	Maximum Percent Difference (LITA vs. CFD)
1	0.00	4.30	1.91	6.15
2	0.05	3.76	0.11	5.69
3	0.94	4.11	0.18	6.57
4	0.34	6.60	0.16	3.24
5	2.92	7.92	1.29	2.60
6	0.24	14.36	0.16	12.15
7	0.04	5.26	0.88	9.13
8	0.61	7.44	0.78	8.24

Table 1. Percent Difference: LITA versus PIV and LITA versus CFD

and Station 2 (x = -6.35 mm), respectively. Overall, LITA shows very good agreement with PIV and CFD, although CFD predicts a higher velocity over most of the profile. The largest percent difference between the LITA and PIV measurements occurs near the model surface where the PIV data is affected by surface flare. The differences between LITA and CFD are greatest near the model and decrease with distance away from the model. In fact, the percent difference between LITA and CFD calculated at Station 2 and y = 60 mm is 0.11%. The lower velocities measured by the experimental techniques are believed to be due to slight differences in the angle of attack between the experiment and the computations as well as three dimensional effects that cannot be accounted for in the two-dimensional computations. Although the effect of the three-dimensionality was most prominent over the flap in the experiment, it can cause a reduction in the suction on the slat. This was seen in comparisons between pressures measured by Paschal, et. al.[24] and the CFD solution, where pressures on the slat upper surface matched CFD when sidewall blowing was used to control the three-dimensional flow but differed by 20 percent when sidewall blowing was not used.
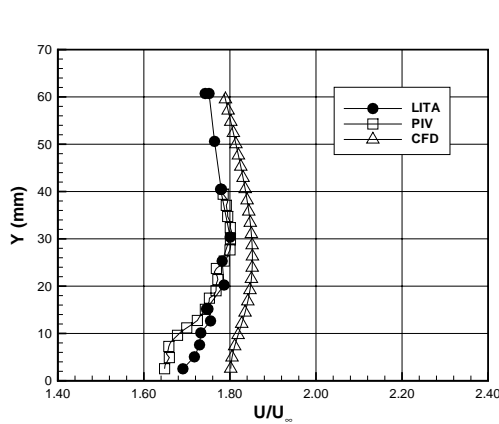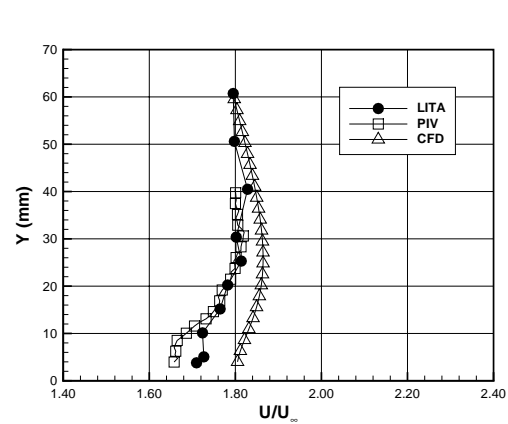

Figure 6. Velocity profiles at Station 1 (x = -7.39 mm)

Figure 7. Velocity profiles at Station 1 (x = -6.35 mm)

4.2 Slat Wake

Figures 8, 9, and 10 show profiles of the normalized, streamwise velocity obtained at Station 3 (x = 6.35 mm), Station 4 (x = 25.40 mm), and Station 5 (x = 50.40 mm). At these locations, the slat wake has formed and converges with flow accelerating around the leading edge of the main element. Figure 8 shows profiles starting just above the wake and extending away from the body. Although the velocities measured by LITA are lower than the PIV, the differences are within the measurement uncertainty of each technique. This is also true for the differences between LITA and CFD
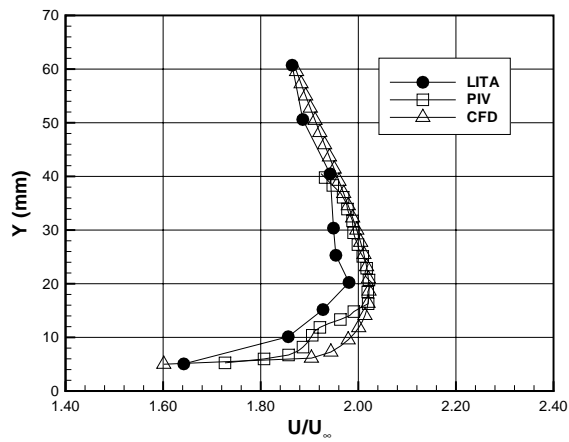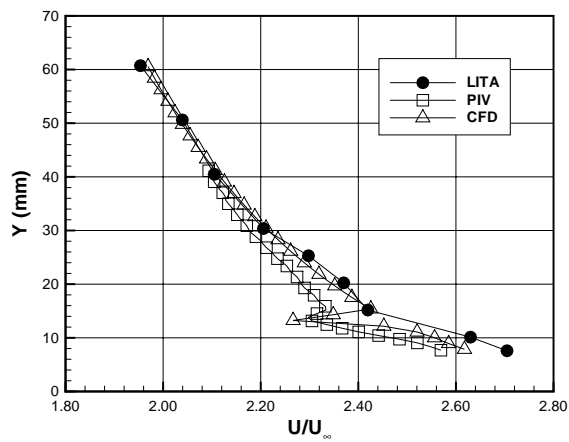
Figure 8. Velocity profiles at Station 3 (x = 6.35 mm).

Figure 11. Detailed velocity profiles at Station 6.
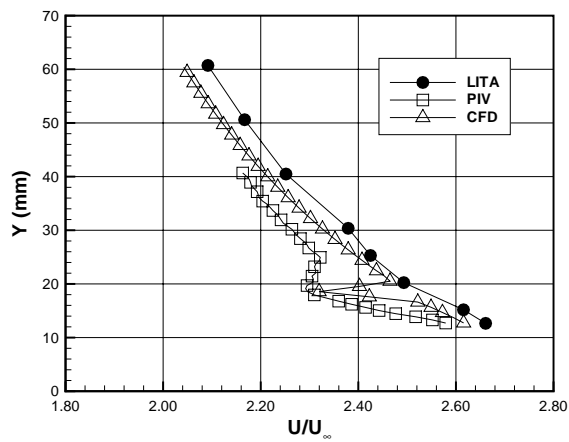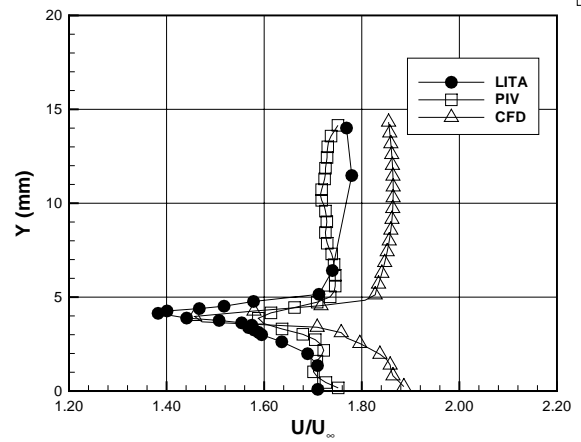

Figure 9. Velocity profiles at Station 4 (x = 25.40 mm).

Figure 12. Detailed velocity profiles at Station 7.

Figure 10. Velocity profiles at Station 5 (x = 50.80 mm).

Figure 13. Detailed velocity profiles at Station 8.

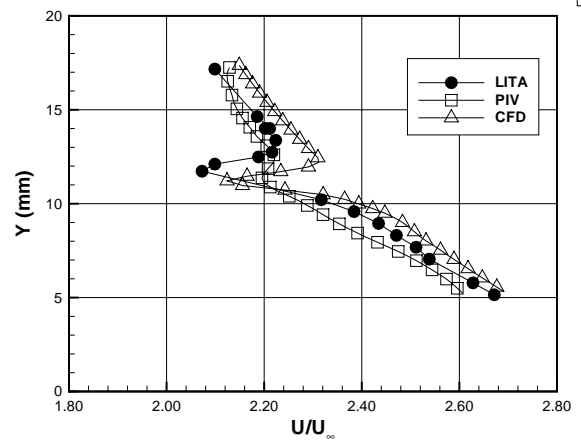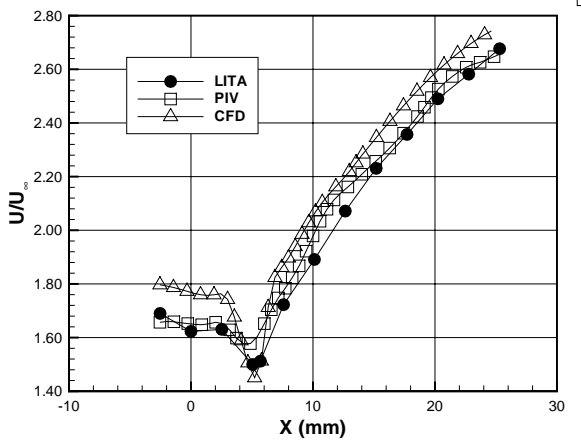except below y = 20 mm. Between y = 20 mm and y = 8 mm, the experimental profiles show an inflection that is not evident in the computational profile. Despite its proximity to the model, there is no apparent physical explanation for this feature and additional analysis is required to determine its origin.

At the downstream locations (Figures 9 & 10), LITA resolves the velocities above and below the slat wake but does not capture the velocity deficit seen in the PIV and CFD profiles. This can be explained using Figure 5 where the LITA measurement locations are superimposed over the wake boundaries (dotted lines) approximated from the PIV data. From this figure it is evident that the number of measurement points within the shear layer is too sparse to resolve the velocity gradients and deficit within the shear layer. The LITA and PIV profiles in Figure 10 also show differences well above the measurement uncertainty of the two techniques. These differences are possibly due to unsteady structures in the wake and their effect on the instantaneous velocity.

4.3 Slat Wake Detail

Although the velocity deficit from the slat wake was not evident in the profiles at Stations 3-5, the ability of LITA to characterize this region is clearly shown in Figures 11-13. At Stations 6-8, measurement points were clustered within the wake as shown in Figure 5. Despite sometimes significant differences between the techniques, the qualitative agreement is remarkable. Each of the profiles shows the vertical thickness of the wake to be approximately 3 mm. The large differences shown in Table 1 at Station 6 occur in the center of the shear layer where the velocity deficit measured by LITA is much greater than that measured by PIV and predicted by CFD. In this application, the LITA system's spatial resolution of 300 μm compared to the PIV sample volume of 1.44 mm may account for its ability to resolve the wake in greater detail. Possible reasons for the differences between LITA and CFD include wake unsteadiness, limitations of turbulence modeling, and the neglect of three-dimensionality in the CFD solution.

5.   SUMMARY AND CONCLUSIONS

A study has been conducted to determine the ability of Laser-Induced Thermal Acoustics (LITA) to measure the flow field of a complex aerodynamic system such as a high-lift slat configuration. LITA measurements in 8 locations along the slat were compared with Particle Image Velocimetry experimental measurements and Computational Fluid Dynamics calculations. The normalized data show good agreement where the number of measurement locations has sufficient density to capture pertinent flow phenomena. This study demonstrates the feasibility of using LITA to measure complex off-body flow fields without particulate seeding.

ACKNOWLEDGEMENTS

REFERENCES

1. R. G. Bradley, "CFD Validation Philosophy," *Validation of Computational Fluid Dynamics*, AGARD-CP-437, Vol. 1, May 1988, pp. 1.1-1.6.
2. R. C. Hart, R. J. Balla, G. C. Herring, and L. N. Jenkins, "Seedless Laser Velocimetry Using Heterodyne Laser-Induced Thermal Acoustics," ICIASF, 2001.
3. H. J. Eichler, P. Gunter, and D. W. Pohl, *Laser-Induced Dynamic Gratings*, Springer-Verlag, 1986.
4. E. B. Cummings, "Laser-Induced Thermal Acoustics: Simple Accurate Gas Measurements," *Opt. Lett.* **19**, 1994, p. 1361.
5. E. B. Cummings, H. G. Hornung, M. S. Brown, and P. A. Debarber, "Measurement of Gas-Phase Sound Speed and Thermal Diffusivity Over a Broad Pressure Range Using Laser-Induced Thermal Acoustics," *Opt. Lett.* **20**, 1995, p. 1577.
6. E. B. Cummings, I. A. Leyva, and H. G. Hornung, "Laser-Induced Thermal Acoustics (LITA) Signals From Finite Beams", *App. Opt.* **34**, 1995, p. 3290.
7. A. Stampanoni-Panariello, B. Hemmerling, and W. Hubschmid, "Temperature Measurements in Gases Using Laser Induced Electrostrictive Gratings," *App. Phys.* B **67**, 1998, p. 125.

8. R. C. Hart, R. J. Balla, and G. C. Herring, "Non-resonant Referenced Laser-Induced Thermal Acoustics Thermometry in Air," *App. Opt.* **38**, 1999, p. 577.

9. R. C. Hart, R. J. Balla, and G. C. Herring, "Optical Measurement of the Speed of Sound in Air Over the Temperature Range 300 – 650 K," *J. Acoust. Soc. Am*. **108**, 2000, p. 1946.

10. M. S. Brown and W. L. Roberts, "Single Point Thermometry in High-Pressure Sooting, Premixed Combustion Environments," *J. Propulsion and Power* **15**, 1999, p. 119.

11. P. F. Barker, J. H. Grinstead, and R. B. Miles, "Single-Pulse Temperature Measurement In Supersonic Air Flow With Predissociated Laser-Induced Thermal Gratings," Opt. Comm. **168**, 1999, p. 177.

12. D. J. W. Walker, R. B. Williams, and P. Ewart, "Thermal Grating Velocimetry," *Opt. Lett.* **23**, 1998, p. 1316.

13. S., Schlamp, E. B., Cummings, and H. G., Hornung, "Beam Misalignments And Fluid Velocities In Laser-Induced Thermal Acoustics," *App. Opt.* **38**, 1999, p. 5724.

14. S. Schlamp, E. B. Cummings, and T. H. Sobota, "Laser-Induced Thermal-Acoustic Velocimetry with Heterodyne Detection," *Opt. Lett.* **25**, 2000, p. 224.

15. D. N. Kozlov, B. Hemmerling, and A. Stampanoni-Panariello, "Measurement Of Gas Jet Flow Velocities Using Laser-Induced Electrostrictive Gratings," *App. Phys.* B **71**, 2000, p. 585.

16. B. Hemmerling, D. N. Kozlov, and A. Stampanoni-Panariello, "Temperature and Flow-Velocity Measurements By Use Of Laser-Induced Electrostrictive Gratings," *Opt. Lett.* **25**, 2000, p. 1340.

17. R. C. Hart, R. J. Balla, and G. C. Herring, "Simultaneous Velocimetry And Thermometry Of Air By Use Of Nonresonant Heterodyned Laser-Induced Thermal Acoustics," *App. Opt.* **40**, 2001, p. 965.

18. S. Rozouvan, and T. Dreier "Polarization-dependent laser-induced grating measurements," *Optics. Letters*. Vol. **24**, 1999, p. 1596.

19. R. C. Hart, G. C. Herring, and R. J. Balla, "Common-Path Heterodyne Laser-Induced Thermal Acoustics For Seedless Laser Velocimetry," *Optics Letters*, Vol. **27**, Issue 9, May 2002, p. 710.

20. W. L. Sellers and S. O. Kjelgaard, "The Basic Aerodynamic Research Tunnel – A Facility Dedicated to Code Validation, AIAA-88-1997, May 1988.

21. A. E. Washburn, "The Effect of Freestream Turbulence on the Vortical Flow over a Delta Wing," Master of Science Thesis, George Washington University, 1990.

22. L. N. Jenkins, "An Experimental Investigation of the Flow Over a Notchback Automobile Configuration," Master of Science Thesis, George Washington University, 1999.

23. S.M. Klausemeyer, M. Papadakis, and J.C. Lin, "A Flow Physics Study of Vortex Generators on A Multi-Element Airfoil," AIAA 96-0548, January 1996.

24. K.Paschal, L. Jenkins, and C. Yao, "Unsteady Slat-Wake Characteristics of a High-Lift Configuration," AIAA-2000-0139, January 2000.

25. L. M. Lourenco and A. Krothapalli, "True Resolution PIV: A Mesh-Free Second Order Accurate Algorithm," Proceedings of the 10th International Symposium on Application Techniques in Fluid Mechanics, Lisbon, July 2000.

26. J. Thomas, S. Krist, and W. Anderson, "Navier-Stokes Computations of Vortical Flows over Low Aspect-Ratio Wings," *AIAA Journal*, Vol. 28, No. 2, pp. 205-212, 1990.

27. F. Menter, "Improved Two-Equation k-ω Turbulence Models for Aerodynamic Flows," NASA TM 103975, 1992.